REPORT DOCUMENTATION PAGE

Form Approved
OMB No. 0704-0188

1. REPORT DATE *(DD-MM-YYYY)*	2. REPORT TYPE	3. DATES COVERED *(From - To)*
01-07-2008	Final	Aug 2007 to April 2008

4. TITLE AND SUBTITLE
2.3 Micron High Power Continuous Wave Diode Laser Arrays

5a. CONTRACT NUMBER
FA9550-05-C-0043

5b. GRANT NUMBER
NA

5c. PROGRAM ELEMENT NUMBER
NA

6. AUTHOR(S)
Dr. David Westerfeld

5d. PROJECT NUMBER
NA

5e. TASK NUMBER
NA

5f. WORK UNIT NUMBER
NA

7. PERFORMING ORGANIZATION NAME(S) AND ADDRESS(ES)
Power Photonic Corporation
25 Health Sciences Drive
Stony Brook, N.Y. 11790

8. PERFORMING ORGANIZATION REPORT NUMBER
AFOSR-Final

9. SPONSORING/MONITORING AGENCY NAME(S) AND ADDRESS(ES)
AF OFFICE OF SCIENTIFIC RESEARCH
875 NORTH RANDOLPH STREET ROOM 3112
ARLINGTON VA 22203

10. SPONSOR/MONITOR'S ACRONYM(S)
AFOSR

11. SPONSOR/MONITOR'S REPORT NUMBER(S)
NA

12. DISTRIBUTION/AVAILABILITY STATEMENT
UNLIMITED

13. SUPPLEMENTARY NOTES
NA

14. ABSTRACT

The goal of this project has been the creation of high power laser diode arrays emitting at 2.3 μm. We have achieved that goal with the design fabrication and characterization of laser bars with unprecedented output power and brightness. We have demonstrated quasi-continuous (qCW) wave output powers of 16.7 W from a single 4 mm laser bar. An initial slope efficiency of 0.235 W/A and a threshold current of 6.9 A were demonstrated. Scaled to the industry standard 10 mm laser bar length, this device would have produced 41.75 W of qCW output power at 18 °C. This report identifies the key advancements made during the course of this research effort.

15. SUBJECT TERMS
lasers, mid infrared, threshold current, efficiency

16. SECURITY CLASSIFICATION OF:			17. LIMITATION OF ABSTRACT	18. NUMBER OF PAGES	19a. NAME OF RESPONSIBLE PERSON
a. REPORT	b. ABSTRACT	c. THIS PAGE			Dr. David Westerfeld
U	U	U	SAR	39+cover	19b. TELEPHONE NUMBER *(Include area code)* 631-632-1358

Final Report for Phase II STTR

2.3 Micron High Power Continuous Wave Diode Laser Arrays

Contract: FA9550-05-C-0043

July 2008

Power Photonic Corporation
25 Health Sciences Drive, Box 111
Stony Brook, NY 11790-3350
Principal Investigator: David Westerfeld

Table of Contents:

1 Project Objectives:

The goal of this project has been the creation of high power laser diode arrays emitting at 2.3 μm. We have achieved that goal with the design fabrication and characterization of laser bars with unprecedented output power and brightness. We have demonstrated quasi-continuous (qCW) wave output powers of 16.7 W from a single 4 mm laser bar. An initial slope efficiency of 0.235 W/A and a threshold current of 6.9 A were demonstrated. Scaled to the industry standard 10 mm laser bar length, this device would have produced 41.75 W of qCW output power at 18 °C.

This report identifies the key advancements made during the course of this research effort.

2 Heterostructure development:

We have made several advances in the design of the 2.3 μm laser heterostructure to decrease threshold current and improve efficiency. The following sections describe modeling and experimental work intended to decrease optical loss and improve transport through the separate confinement region (SCR) of the laser structures.

2.1 Optimization of p-cladding doping profile

Figure 1 shows the band (solid lines) and doping (dashed lines) profiles of our Phase I laser. The red line shows the calculated distribution of the optical mode amplitude. There is a noticeable overlap between the optical mode profile and the highly-doped part of the p-cladding layer. This overlap contributes to a total optical loss of about 20 cm^{-1}. Assuming 5% / 95% mirror reflectivities, the internal optical loss is 5-6 cm^{-1}. Since the main source of the optical loss is the highly-doped p-clad region, we can reduce the loss by reducing the doping in this part of the p-cladding layer. Figure 2 shows the calculated percentage of the internal optical loss decrease and the related increase in cladding resistance due to the increased length of the low-doped region *d*. Assuming a p-clad hole mobility of 100 $cm^2/V{\cdot}s$, we obtain the cladding resistance of 3.5 milliohm in the older

device. This allows us to safely extend the low-doped region to 0.5 μm, which should decrease the internal loss to 3 cm^{-1} with a cladding resistance of only 4 milliohm.

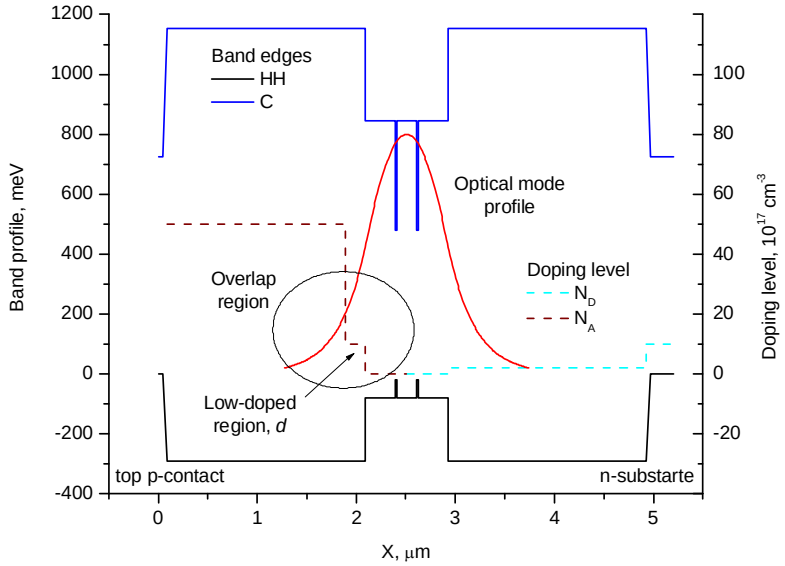

Figure 1: Band edges and doping profiles of the laser heterostructure. Red indicates the optical mode intensity profile. The area of optical mode overlap with the doped p-cladding is circled

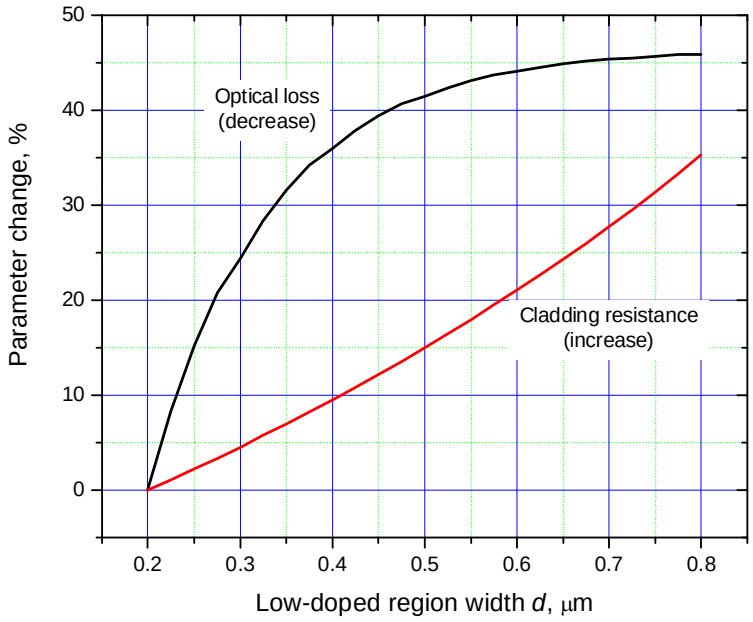

Figure 2: Relative changes in p-cladding resistance (red) and internal optical loss (black line) vs. the length of low-doped part of the p-cladding.

2.2 Design of the SCR-cladding graded regions

Band discontinuities at the heterointerfaces between the separate confinement region (SCR) and the cladding regions can be efficiently smoothed by replacing the abrupt interface with a specially designed compositionally graded transition region with modulation doping [1]. Smoothing the band discontinuities not only reduces the laser threshold voltage but also improves the conditions for carrier injection into the SCR. This implies elimination of strong local electric fields usually associated with abrupt heterobarriers and, therefore, (i) reduces local heat generation at the SCR-cladding heterojunctions, and (ii) eliminates hot carrier injection into the SCR. The later also reduces temperature-induced gain degradation in the laser active region and helps reduce active region overheating.

Grading the heterojunction between the cladding and SCR is complicated by the lack of certainty in the X and L valley ordering in quaternary $Al_xGa_{1-x}As_ySb_{1-y}$ alloys. Provided the X-to-L(Γ) transition occurs at $x_{tr} = 0.14$ due to strong X valley bowing as predicted

by the latest theoretical calculations [4], a smooth linear or quadratic grading from x = 0.9 to x = 0.25 would be appropriate for the cladding / SCR interface. We take the simpler approach of stepwise grading with three transition layers, x = 0.35, x = 0.5, and x = 0.75. The layer with the first composition ensures interface smoothing in the absence of pronounced X bowing. The second layer corresponds to an alternative value of X-to-L(Γ) transition concentration x_{tr} [5] while the last composition provides interface smoothing in case of large X valley bowing predicted in [4].

Figure 3 shows the band profiles of the n-cladding/SCR region and the corresponding quasi-Fermi levels for three different types of transition grading at an external bias compensating the build-in potential $V_{bi} = 0.65V$. The black lines show the profiles without grading, the red ones correspond to a three-step grading design, and the blue lines illustrate the ideally smooth linear band grading. The later is shown for comparison purposes. The n-doping is interrupted in the middle of smooth graded region or at the interface between the first two (x = 0.35, 0.5) and the third (x = 0.75) grading steps to allow for additional band profile smoothing due to the charge transfer. Note that the quasi-Fermi levels in both types of graded regions are nearly continuous which indicates the absence of noticeable thermionic current between layers. The modeling shows that simple three-step design efficiently enhances the electron injection through the cladding / SCR interface region. Figure 4 shows calculated I-V characteristics of a diode for the three types of transition grading considered above. It is readily seen that three-layer grading design is nearly as efficient as an ideally smooth linear band-edge grading.

Figure 5 shows similar calculations for the p-cladding/SCR transition region. As expected, the diode I-V characteristic does not significantly change with grading of p-cladding/SCR interface; see Figure 4, dashed lines.

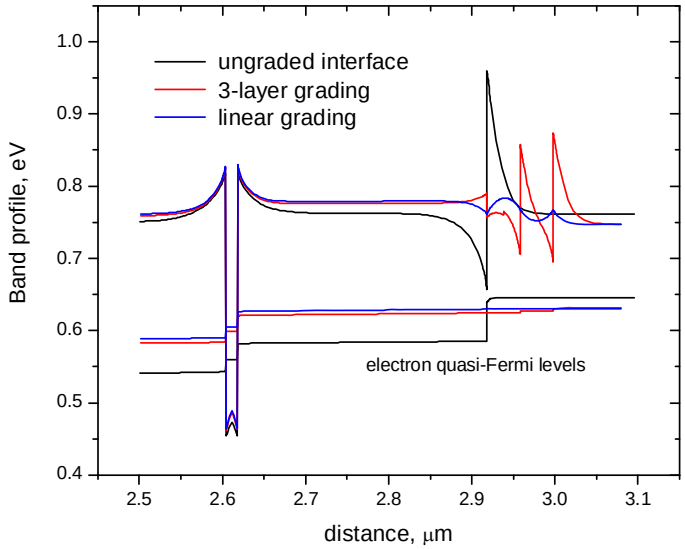

Figure 3: Conduction band profiles for different types of grading of the SCR – n-cladding interface region. Efficient smoothing of the quasi-Fermi levels at the interface by 3-layer grading (compare black and red lines) indicates significant reduction of the thermionic current in the overall injection process.

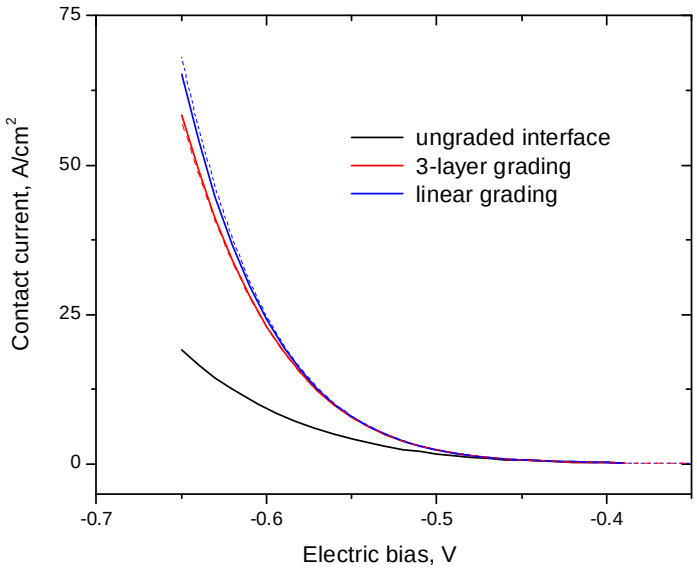

Figure 4: Contact current of the diode structures with different grading of the SCR – n-cladding interface. 3-layer grading demonstrates same level of injection improvement as an idealistic linear

grading (compare red and blue curves). Dashed lines illustrate insignificant role of the p-cladding – SCR interface grading.

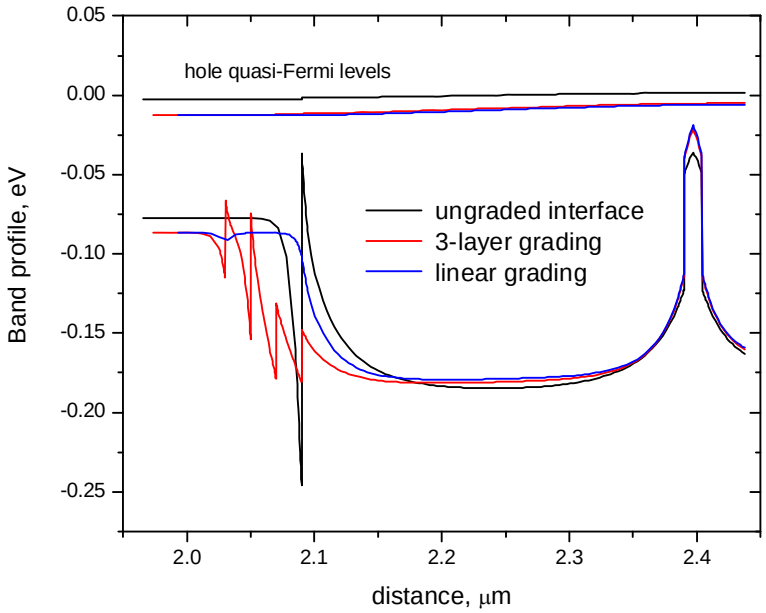

Figure 5: Valence band profiles for different types of grading of the SCR – p-cladding interface region. The small discontinuity of the hole quasi-Fermi level at the ungraded interface indicates the insignificance of the thermionic current in hole injection.

2.3 Design of the SCR selective doping profile and SCR layout optimization

Doping the SCR provides the most natural way to decrease the series resistance and reduce the operating voltage thus increasing the power conversion efficiency. As a bonus, extending the n-doping through the SCR up to the edge of the adjacent quantum well imposes electrostatic barriers for both electrons and holes at the quantum well position which act like stopper layers [2] and help enhancing the carrier capture [3].

Modeling of the diode laser at threshold first requires an estimation of the threshold concentration in the active quantum wells. Active quantum well levels (Figure 6), subband dispersions (Figure 7), electron, hole, and joint density of states (DOS) for optical transitions (Figure 8), and optical gain spectra for different carrier concentrations

in the active quantum wells (Figure 9) have been calculated for this purpose. Subband dispersion and DOS calculation indicate a strong influence of the hole subband nonparabolicity and second hole subband DOS on the hole lasing state filling; see Figure 10. The threshold concentration for a loss value of 17 cm^{-1} was estimated as $N_{th} = 5\times10^{11}$ cm^{-2}; see Figure 9. This value was then used for laser modeling and SCR layer resistance calculations for the different doping profiles.

Figure 11 shows the SCR band profiles with unintentional (residual) SCR p-doping, $N_a = 10^{16}$ cm^{-3}, and also for intentionally n-doped SCR3 layer, which is the layer adjacent to the n-cladding. The doping range was N_d = (1 to 5)$\times10^{16}$ cm^{-3}. All the band profiles have been calculated at the threshold voltage, which was found to be gradually decreasing from 5.2V for the undoped SCR3 layer to 4.8V for a $N_d = 5\times10^{16}$ cm^{-3} doping level. The threshold profiles do not differ noticeably except for the voltage drop in the SCR3 region, though the corresponding profiles in unbiased structures were quite different throughout the all SCR layers. Figure 12 shows the calculated resistances of the SCR layers versus the SCR3 n-doping level. It is readily seen that the SCR3 layer doping of $N_d = 3\times10^{16}$ cm^{-3} provides the optimum change in the layer series resistance.

A further decrease of the device series resistance can be obtained by narrowing the SCR layer SCR2. Figure 13 shows the calculated resistances of the layers SCR2 and SCR3 vs. the SCR2 layer width at the SCR3 doping level of $N_d = 3\times10^{16}$ cm-^{3}. By decreasing the width of the SCR2 layer down to 100 nm the series resistance of this layer decreases by a factor of three while the quantum well separation still exceeds the strain relaxation length by about an order of magnitude [6]. Further reduction of the SCR2 layer width is not reasonable since the SCR1 resistance becomes the dominant at this point. Figure 14 shows the corresponding changes in the conduction band profile of the structure.

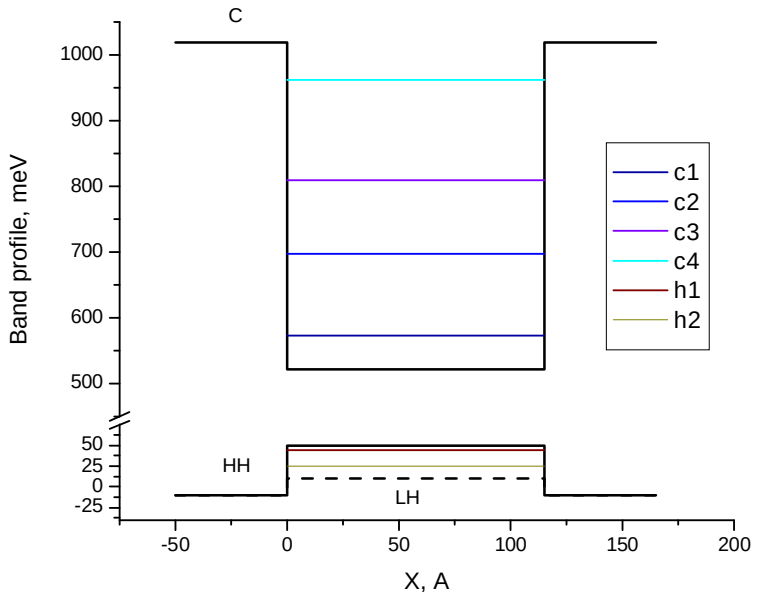

Figure 6: Band profile and electron and hole energy levels in the active quantum well.

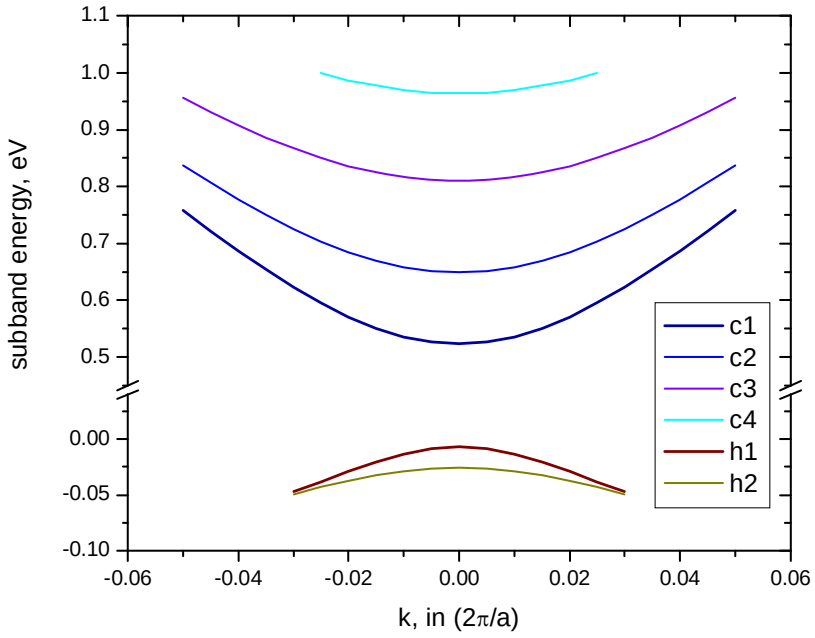

Figure 7: Subband dispersion and non-parabolicity.

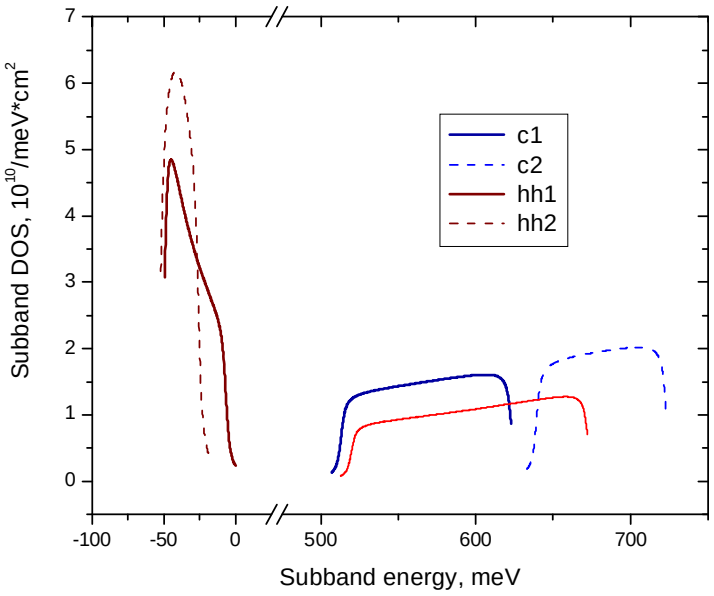

Figure 8: Density of states (DOS) for subband participating in lasing transition (solid lines). Dashed lines show DOS for next higher-laying subbands. Note the strong nonparabolicity and narrow separation of the hole subbands. The red line shows the joint density of states for the optical transition.

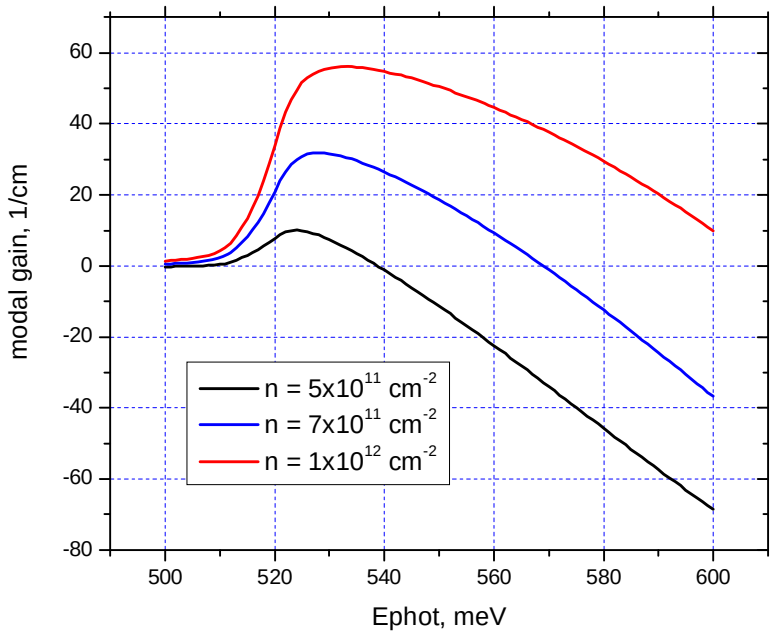

Figure 9: Calculated modal optical gain for different values of carrier concentration in the active quantum well.

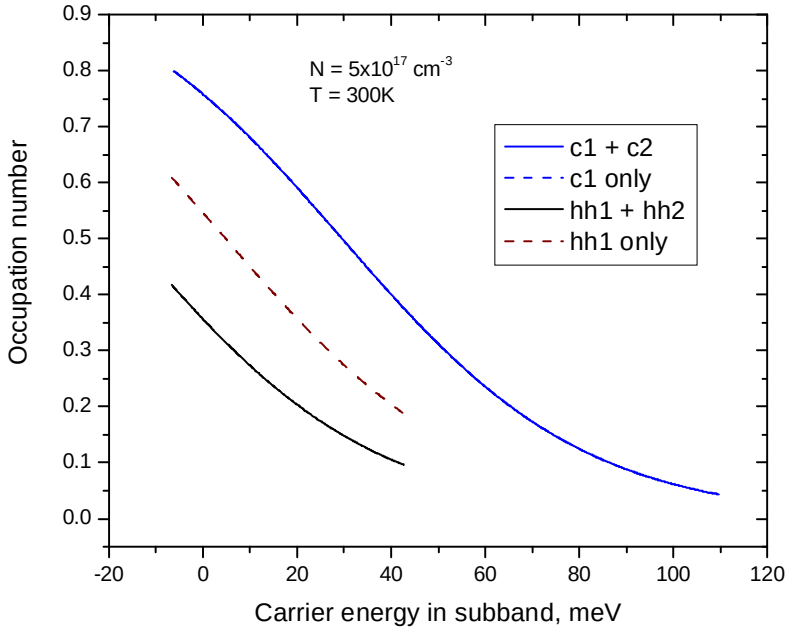

Figure 10: Role of the second (higher-laying) hole subband in the overall hole state population. Solid lines show actual population of the electron (blue) and hole (black) lowest subbands taking into account the effect of the filling of the higher subband states. Dashed lines illustrate the state population without the higher subband presence.

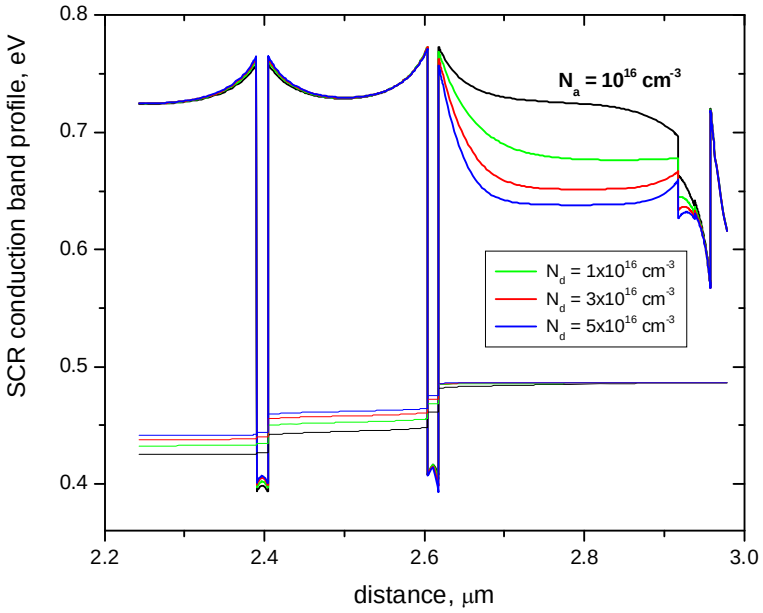

Figure 11: Conduction band profiles of SCR for different levels of the SCR3 layer doping. Profile with $N_a = 10^{16}$ cm^{-3} represents the unintentionally p-doped layer.

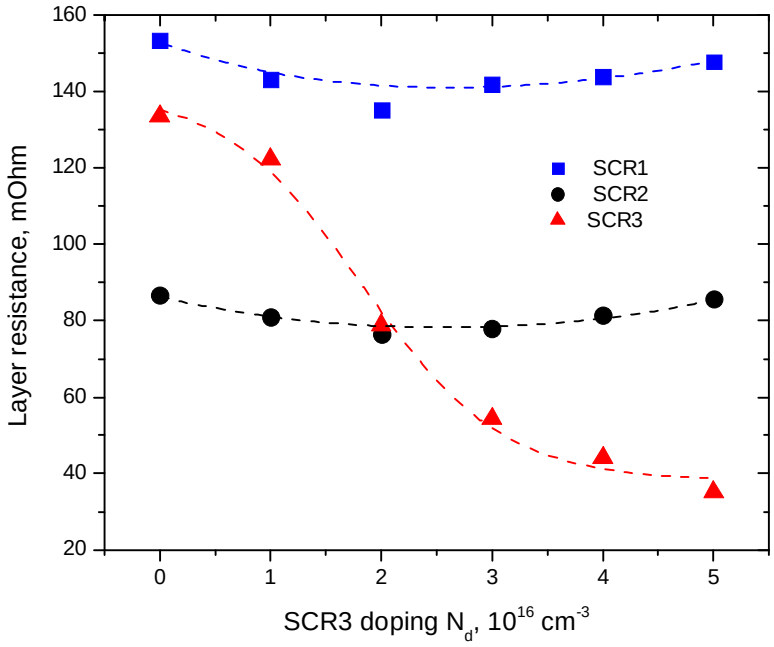

Figure 12: SCR layer resistances vs. doping level of the SCR3 layer.

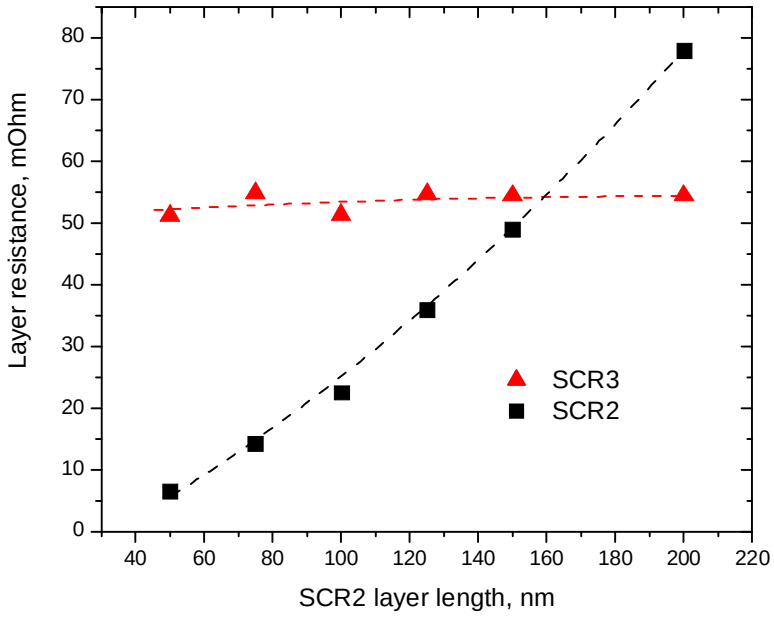

Figure 13: SCR2 and SCR3 layer resistances vs. SCR2 layer length.

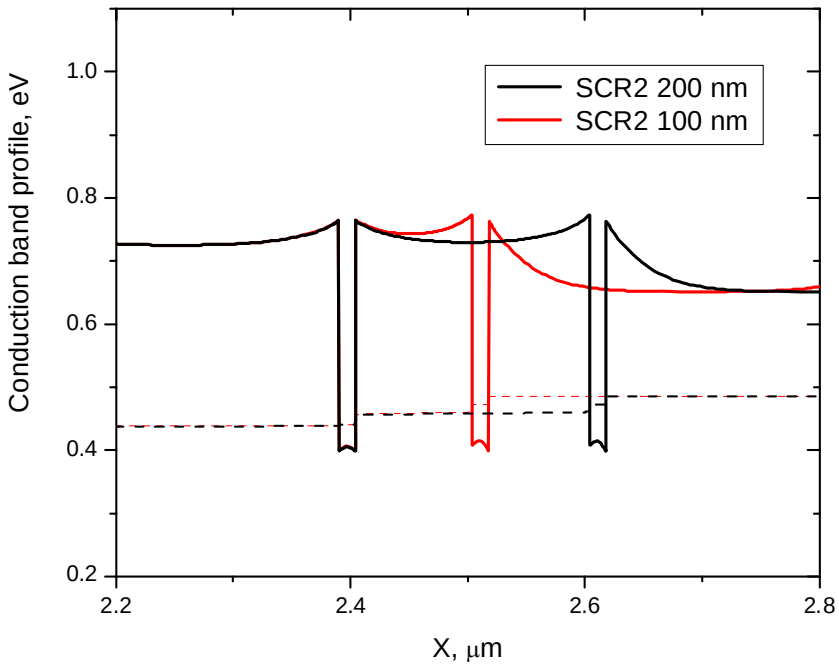

Figure 14: Conduction band profiles for two values of SCR2 layer length, 200 nm (black) and 100 nm (red).

Aside from the technological developments, the research effort has yielded a new laser active region design which has demonstrated a threshold current density reduced to half of our previous devices. Our device modeling procedure was refined to include barrier states in the QW gain calculations; this modification has proven to be crucially important in the active region design.

A comprehensive experimental and theoretical analysis has established a novel approach to the design of GaSb-based high power laser diodes. Additional information about these efforts is included in the Accomplishments / New Finding section.

2.4 Heavily strained active region for high differential gain

We have developed a 2.35 μm QW laser design with low threshold current. Hakki-Paoli modal gain measurements were performed on devices with the new design and lasers of the previous generation. The halving of the threshold current is explained by a more than 3 fold increase in differential gain with respect to current for devices with the new,

heavily strained QW design (Figure 15). An increase of the QW compressive strain from 1.2% (previous design) to 1.6-1.7% (new design) decreases the in-plane heavy hole density of states and thus decreases laser threshold concentration. The heavily strained QWs also have improved hole confinement and a slightly improved carrier lifetime, presumably due to a reduced Auger recombination coefficient. Figure 16 shows the experimental photoluminescence decay curves measured using a photon counting up-conversion technique. At high pumping levels (beginning of the PL decay curve) slower carrier recombination is observed for the structures with new design indicating a reduced Auger recombination rate.

We have also fabricated lasers with four QWs of the new design. Gain measurements show that no advantage in device performance is expected for lasers with four QWs since the differential gain stays the same as the two QW devices, while the higher transparency current of the four QW sample increases the net laser threshold (Figure 15).

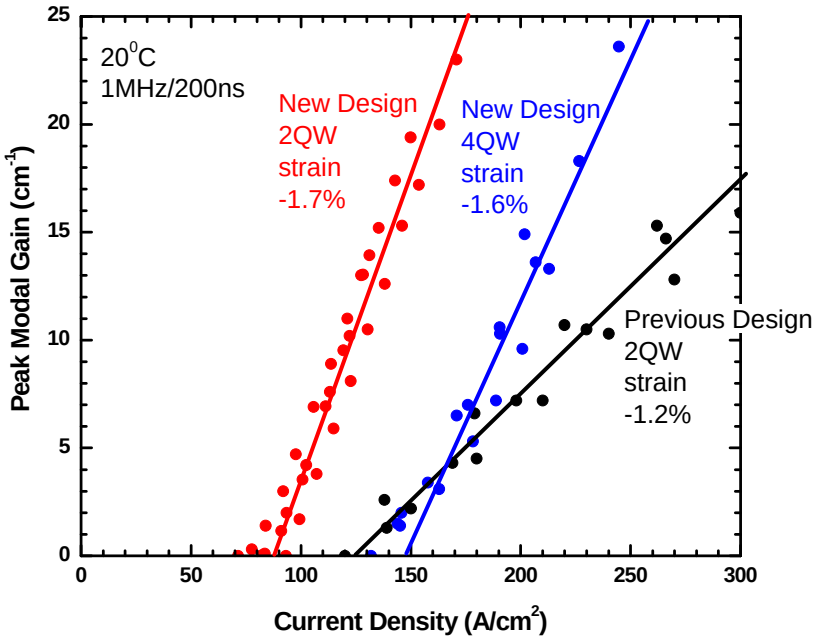

Figure 15: Peak modal gain versus current density for 2QW lasers of new (red) and previous (black) designs, and 4QW lasers of new design (blue).

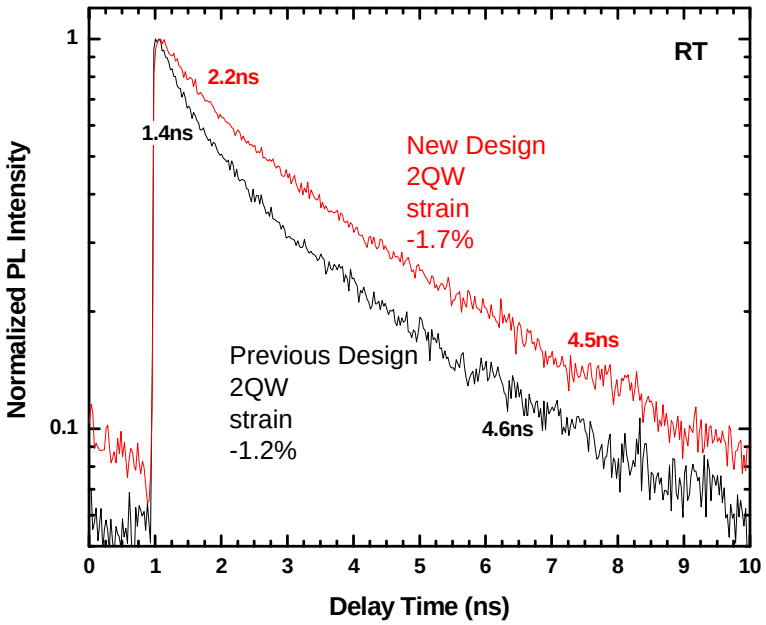

Figure 16: Photoluminescence decays for 2QW laser heterostructures of new (red) and previous (black) designs.

2.4.1 High power lasers with low threshold current

The experimental data presented in section 2.4 demonstrate a trebling of the differential gain for laser structures with heavily strained active regions. The increased strain did not increase the measured optical loss and the carrier lifetime even improved slightly. As a result, lasers with the heavily strained active region have a laser threshold current less than half that of the Phase I lasers; see Figure 17. The CW light-current characteristics of the 1 mm-long laser diode of the new design mounted epi-down on a copper heat sink is shown in Figure 18. *The maximum power level of 700mW sets a new record for 1mm-long 2.3μm high power multimode lasers.*

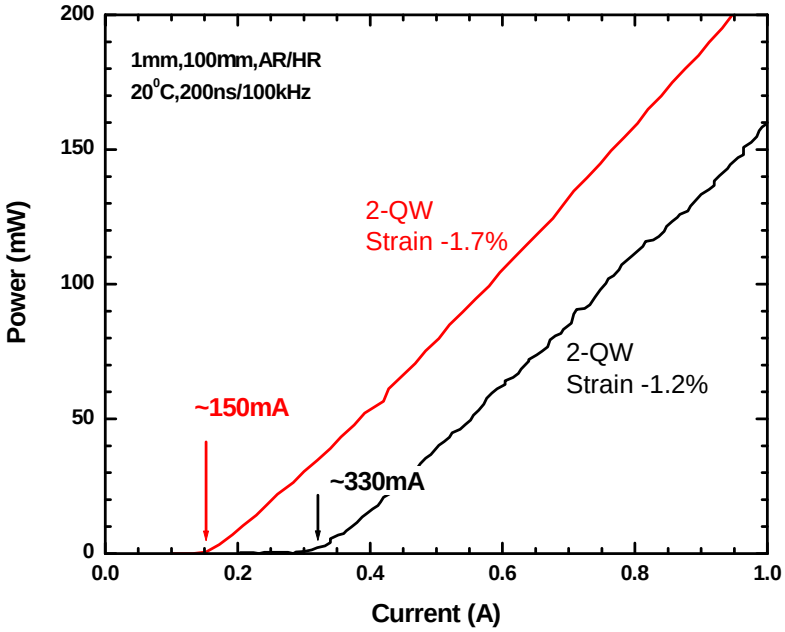

Figure 17: Pulsed light-current characteristics of the lasers with new high strain (red) and previous (black) design of active region.

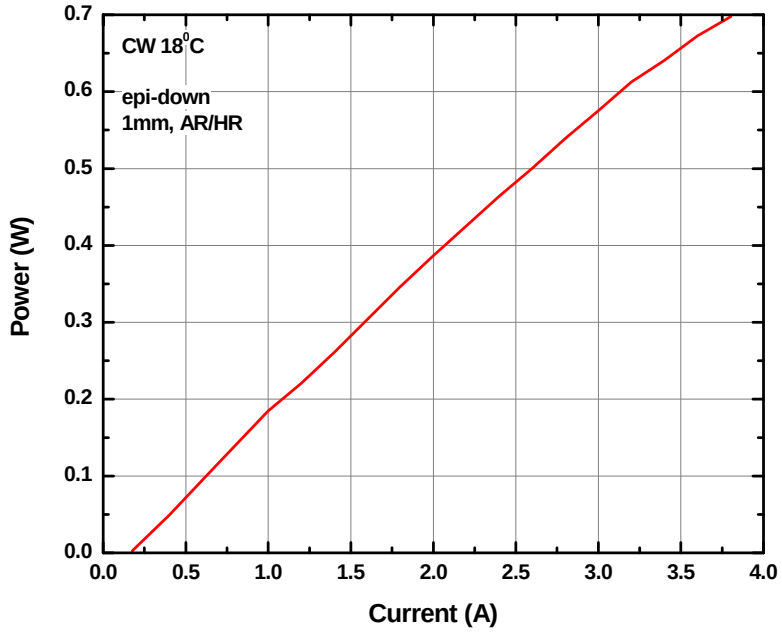

Figure 18: CW Light-current characteristics of the lasers with the heavily strained active region.

2.4.2 Calculation of the modal gain in GaSb strained lasers

We have performed detailed modeling and experimental studies of laser structures characterized by different QW compositions and, accordingly, different strains and different hole confinements. In our calculations, the valence band positions in quaternaries have been obtained by linear interpolation of experimental data for binaries. Active region modeling was accomplished through the development of a COMSOL program based on the 8-band kp-model including strain-induced subband spectrum modification.

Compressive strain splits the first heavy-hole (HH) and first light-hole (LH) subbands thus reducing the edge hole DOS, which otherwise is unfavorably increased by HH-LH subband mixing. Our calculations show that this mechanism of gain improvement works well in GaIn(Al)AsSb QWs only for compressive strain values up to about 1%. Strain beyond ~1% has little additional effect on the edge hole DOS since the LH and HH states are already well separated. We emphasize that the use QW compressive strains above 1% can be crucial for successful fabrication of high power room temperature operated GaSb-based mid-infrared diode lasers. Compressive strain moves the position of the QW valence band edge upwards and makes the hole QW deeper. Improved hole confinement reduces thermally activated population of the inactive QW subbands and the barrier bulk states "saving" holes for the lasing states ultimately enhancing the laser differential gain and reducing the threshold current density. Enhancement of the optical gain in Sb-based laser heterostructures through the strain-induced increase of the hole confinement (hole QW deepening) remains efficient for high compressive strains in the 1%-2% range while preserving the main benefits achieved at the lower strain level – balanced joint DOS and, possibly, reduced Auger recombination rate.

According to our estimation, the depth of the hole QW increases with strain from 42 meV (laser design used in Phase I) to 116 meV (new design). The deepening of the hole QW diminishes the thermal redistribution of the holes and, for the same total carrier concentration, increases the occupation of the upper hole subband participating in lasing transition. Figure 19a shows the calculated hole distribution functions in the laser structures at a fixed carrier concentration: solid lines – taking into account of hole

thermal redistribution between lasing and non-lasing states, dashed lines – ignoring thermal redistribution of holes.

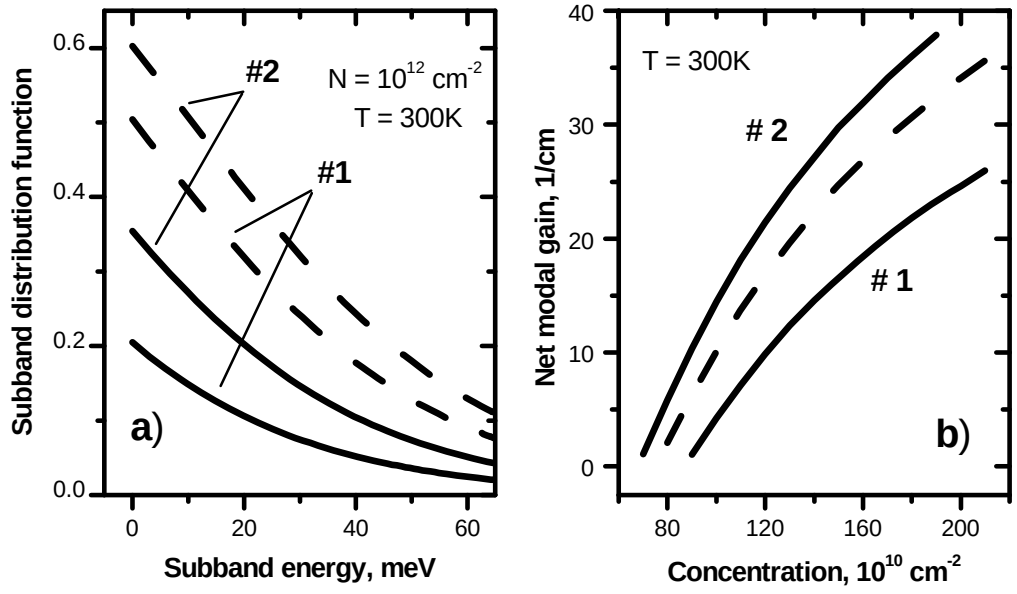

Figure 19: a) Hole distribution functions for structures with previous (#1) and improved (#2) designs. Dashed lines show Fermi distributions in the case when only one hole and one electron subband are present. b) Gain enhancement due to the improved hole confinement: #1 – previous design; #2 – new design with hole confinement enhanced by QW deepening due to strain and composition optimization; dashed line – hole confinement enhanced by a 10% increase of Al contents in barrier layers.

It is readily seen from a comparison of the solid curves 1 and 2 that QW deepening significantly improves the valence band edge occupation. Comparison of the dashed curves 1 and 2 illustrates the role of strain-induced hole DOS reduction. Due to the large conduction band offsets in the In(Al)GaAsSb system, the effect of the compressive strain increase on electron redistribution between higher electron subbands and electron continuum is minor. In In(Al)GaAsSb lasers, the implication of the improved hole confinement for optical gain is straightforward – laser #2 with better hole confinement demonstrates significantly better hole state occupation, higher differential gain, and lower threshold concentration; see Figure 19b. To elaborate on the decisive role of QW deepening in gain enhancement we have additionally modeled a laser structure with the same QW composition as in laser #1 but with higher (35% versus 25%) aluminum

contents in the AlGaAsSb layers. The QW deepening in this case is determined by lower position of the valence band edge in barrier material with higher Al contents. QW composition and QW strain both remain the same. Improved hole confinement again demonstrates distinct gain enhancement in structure with deeper QW; see Figure 19b, dashed line.

3 High strain single emitters:

Laser structures with 1.6% compressive strain in the QWs were grown to verify the high strain laser heterostructure performance (section 2.4). The laser heterostructures were grown on Te-doped GaSb substrates. The cladding layers were 1.5-μm-wide $Al_{0.9}Ga_{0.1}As_{0.07}Sb_{0.93}$ doped with Te (*n* side) and Be (*p*-side). Graded band gap heavily doped transition layers were introduced between the substrate and *n* cladding and between the *p* cladding and *p* cap to assist carrier injection. The nominally undoped $Al_{0.25}Ga_{0.75}As_{0.02}Sb_{0.98}$ waveguide layer with a total thickness of about 800 nm contained two 12-nm-wide $In_{0.37}Ga_{0.63}As_{0.1}Sb_{0.9}$ QWs centered in the waveguide and spaced 20 nm apart. The thick waveguide and cladding layers were lattice matched to GaSb. The wafer was processed with 100-μm-wide oxide confined gain guided stripes. Lasers with 1- and 2-mm-long cavities with antireflection (AR) (~3%) and high-reflection (HR) (~95%) coatings were In-soldered epi side down onto Au-coated polished copper blocks and characterized.

Figure 20 shows the CW light-current and power-conversion characteristics for 1- and 2-mm-long AR/HR coated lasers. A maximum CW output power level above 850 mW was achieved for the 1-mm-long laser at 4 A, while the 2-mm-long device with twice the thermal footprint produced an output of 1.050 W at 6.2 A. The device power-conversion efficiency peaked at 17.5% for the 1 mm-long lasers and was above 10% over the whole range of operation for the 2-mm-long devices.

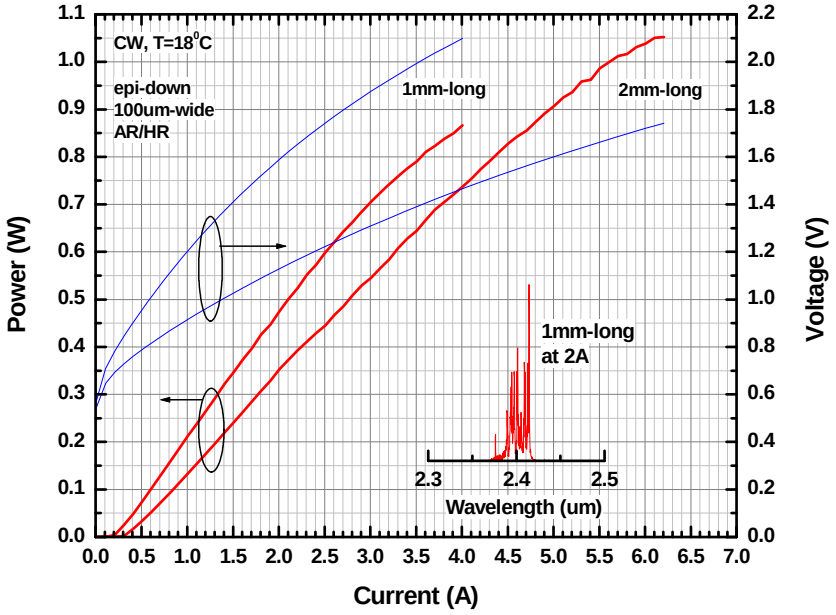

Figure 20: CW current dependences of the output power and power-conversion efficiencies of 2.4 μm AR/HR coated lasers with cavity lengths of 1 and 2 mm. The inset shows the laser spectrum of the 1-mm-long device at 2A.

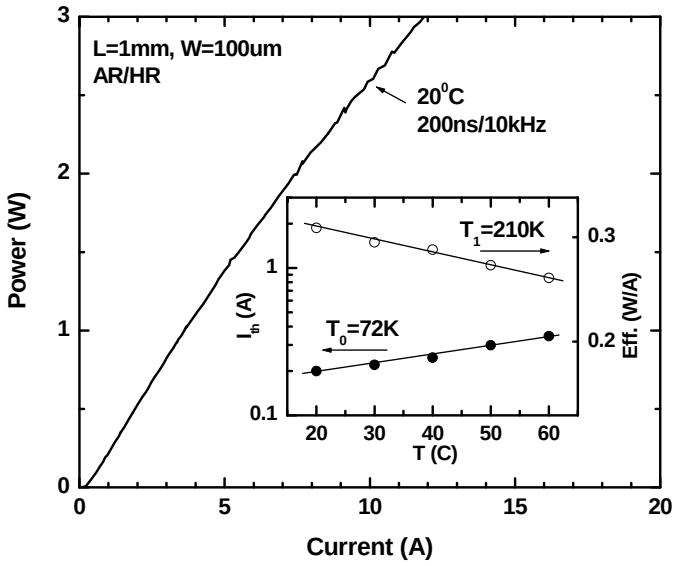

Figure 21: Pulsed light-current current characteristic of 1 mm long AR/HR coated lasers emitting at 2.4 μm. The inset shows the temperature dependences of the laser threshold and slope efficiency.

In short-pulse low duty cycle operation (200 ns/10 kHz), the 1-mm-long devices show no thermal roll over and more than 3 W peak power level was produced at 12 A (Figure 21).

The inset in Figure 21 shows the temperature dependences of the 1-mm-long device threshold current and efficiency. Parameters T_0 and T_1 characterizing the exponential increase of the threshold current and decrease of the external efficiency with temperatures are above 70 and 200 K, respectively.

The devices exhibit high external efficiency and low threshold current density, approximately half that of previous devices. Experiment shows that the low threshold current density correlates with high device differential gain with respect to current. Theoretical analysis suggests that this enhancement of the laser parameters is consistent with the improved hole confinement energies due to the heavily strained active regions.

3.1 Adjustment of the QW material parameters for lasing at 2.3μm

The high strain design of the previous section was modified to bring the emission wavelength to the target of 2.3 μm. A new generation of 2.3-μm laser diodes with superior performance compared to the previously design was obtained by increasing the compressive strain to 1.7%, decreasing the QW thickness down to 9 nm and increasing the Indium composition to 34%.

Figure 22 shows the output power and power conversion efficiency (PCE) for coated lasers described above as functions of CW current. The threshold current of 180 A/cm^2, initial slope efficiency of 0.205 W/A and peak PCE of 15.5% were similar to those reported in [1] for 2-mm-long devices. The PCE in the high-current region was higher than that in [1] which resulted in a smaller thermal roll-off of the output power with current. At the 1-W output power level the PCE remained above 12 %, which is 20 % greater than the corresponding value presented in [1]. A maximum CW output power of 1.15 W was observed from the 2-mm-long devices. A maximum CW power of 850 mW was observed from 1-mm-long devices.

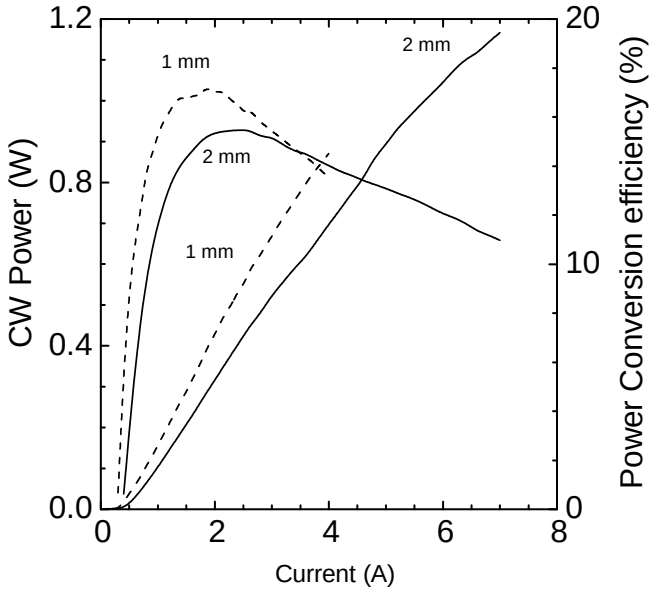

Figure 22: CW current dependences of the output power and power-conversion efficiencies of the AR/HR coated lasers with the cavity lengths of 2 mm (solid lines) 1 mm (dashed lines). The laser characteristics were measured at a heat sink temperature of 18^0C.

Figure 23 shows the lateral cross-section of the laser near-field image recorded using a mid-IR camera. The near-field image revealed 6 filaments with an average spacing of 20 μm. An increase of the filament spacing compared to that in the 2.3-μm lasers with ~1 % compressive strain was observed. This increase correlates with the improved differential gain expected due to the increased compressive strain.

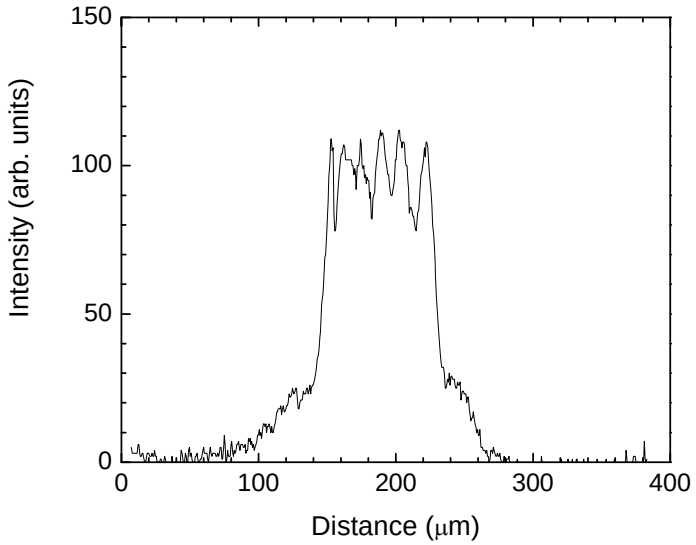

Figure 23: The near-field image of the 2.3 μm diode lasers.

The emission spectrum and tuning of the emission spectrum center as a function of current under CW operation are shown in Figure 24. The devices were tested in the quasi-continuous wave (qCW) mode (Figure 25) under 30-μs-long current pulses with a repetition frequency of 300 Hz. The maximum qCW power of 1.4 W was obtained at a current of 8.5 A. The voltage drop across the laser heterostructure was below 1.5 V all the way up to 8 A.

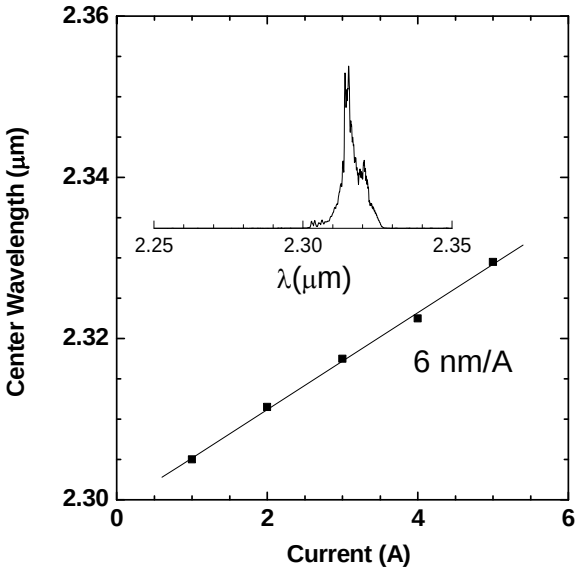

Figure 24: The emission spectrum and tuning of the emission spectrum center for 2-mm lasers tested at CW. The tuning rate with current was found to be 6 nm/A.

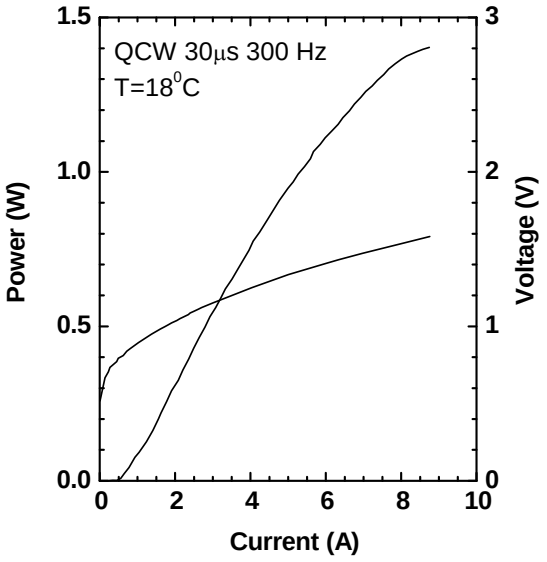

Figure 25: Quasi-CW power (30 μs pulse width, 300 Hz repetition rate) and voltage–current characteristics of 2-mm lasers obtained at a heat sink temperature of 18°C.

4 Growth development:

The exit of our original subcontractor, Sarnoff Corporation, from GaSb growth field led us to create our own growth facilities at Stony Brook University. A Veeco GEN-930

solid source molecular beam epitaxy machine was specified, ordered, built, installed, and validated in a newly renovated building on the Stony Brook campus. We have demonstrated the growth of high quality 2.3 μm laser material using this state of the art facility. Devices developed and fabricated using these new technological capabilities outperformed the previously reported lasers.

4.1 Development of in-house material growth and device fabrication

Figure 26 shows the newly acquired GEN-930 solid source molecular beam epitaxy (MBE) system installed and operated at Stony Brook University. This machine is dedicated to GaSb-based photonic device development. Figure 1.2 shows the photoluminescence (PL) intensity from a laser heterostructure grown at Stony Brook (red) in comparison to the one that was grown by our Phase-I subcontractor. Figure 27 shows the substantial improvement in PL intensity in the SUNY-grown laser structure as compared to the previous one. The observed PL intensity improvement is related increased material quality and efficiency of the active region. Figure 28 shows the X-ray rocking curve measured for the 2.3 μm laser heterostructure grown at SUNY.

Figure 26: Veeco GEN-930 solid source molecular beam epitaxial growth machine

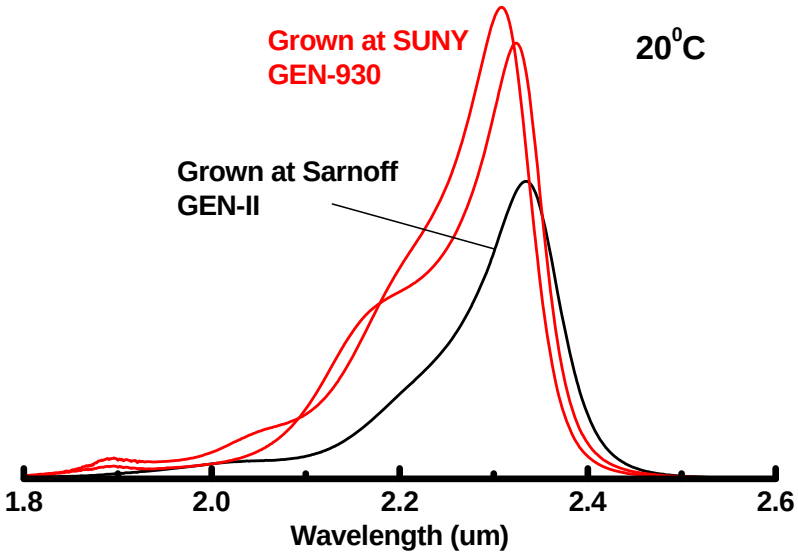

Figure 27: Room temperature photoluminescence spectra of the laser structures grown recently at SUNY (red) and grown previously at Sarnoff (black). The latter structure was used to fabricate linear laser array with 10W CW.

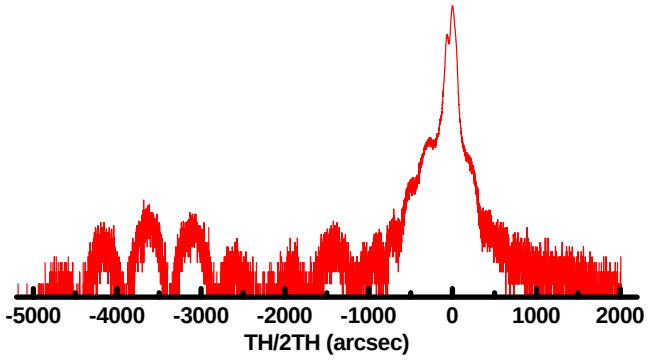

Figure 28: X-ray rocking curve of the laser heterostructure grown at SUNY.

The measured PL spectrum and X-ray characterization demonstrates the high quality of the new SUNY/PPC technological capabilities. The SUNY-grown laser structures were in-house processed into 100 μm-wide 1-mm long laser emitters. Figure 29 shows pulsed light-current characteristics for 1-mm-long uncoated laser diodes. These devices demonstrate an external efficiency of about 55% and a threshold current density of about 150 A/cm^2. These results indicate that satisfactory GaSb growth capability has been established at Stony Brook.

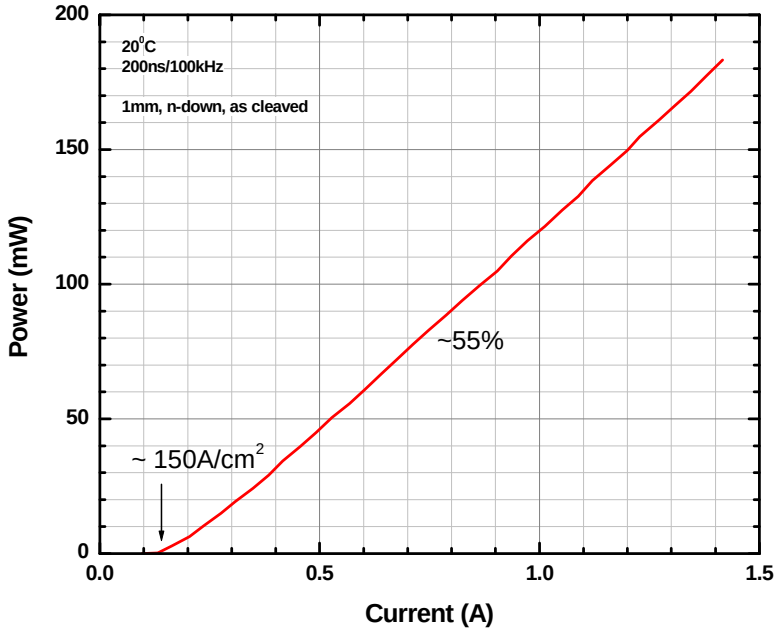

Figure 29: Light-current characteristics of the SUNY-grown and SUNY-processed laser diodes.

4.2 Upgrade of the MBE sources to SUMO cells

The solid-source molecular beam epitaxy (MBE) system has been upgraded, replacing the single-filament Gallium and Aluminum sources with two-heating zone SUMO sources and the addition of a second Aluminum source (also of the SUMO type). The SUMO sources offer better flux stability over time, better spatial homogeneity and, of special importance, a reduction in the oval defect concentration. The addition of the second Al source allows us to obtain improved heterointerfaces between alloys having greatly different Al compositions (i.e., clad/SCH) by reducing the growth interruption.

5 Development of 2.3 μm laser diode arrays:

The advanced high strain heterostructure utilized in the individual lasers of section 3.1 was applied to the next generation of Type-I GaSb-based laser diode arrays. The reduction of the threshold current density allowed for an increased array fill-factor (FF) for a higher power output. Previous estimations showed that the parasitic laser generation in the lateral direction should not occur in arrays with a fill-factor (FF) of up to 30 %. Thus, 30% FF laser diode arrays with standard overall widths of 10 mm and cavity

lengths of 1 mm and 2 mm were fabricated and tested. The voltage-current and power-current characteristics of the 2-mm-long array are shown in Figure 30.

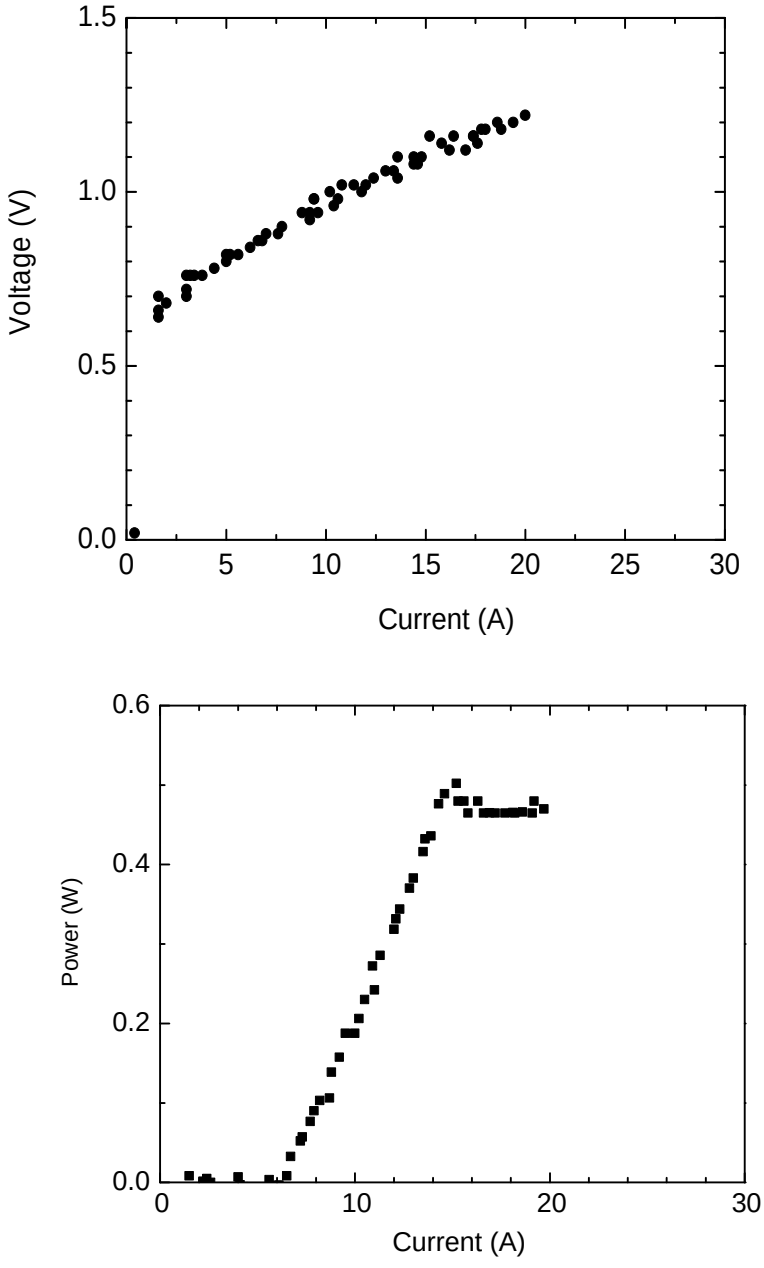

Figure 30: (top) Voltage–current characteristic of the 2x10 mm laser diode array with 30% fill-factor; (bottom) CW power of the same array. The characteristics were measured with arrays mounted p-side down on water-cooled heat sinks with 18°C water temperature.

A decrease of the voltage drop across the devices was observed as expected, however both the 1-mm and 2-mm devices demonstrated saturation of the output power with

current after certain levels due to bleaching of the unpumped regions between the laser stripes leading to generation of lateral modes with low mirror loss. The power-current characteristic of the 2-mm device showed saturation at a power level of 0.5 W. A saturated output power of only ~100 mW was observed for the 1-mm devices. Clearly, our original estimation that a 30% fill factor array would be safe from lateral lasing was incorrect.

In order to suppress the lateral mode generation, a new wafer with grooves between the laser stripes was processed. The grooves increase the loss for the parasitic lateral lasing modes, while not affecting the desired longitudinal modes. A photo of the wafer with grooves is shown in Figure 31. Figure 32 shows the groove depth profile measured with a stylus profile meter.

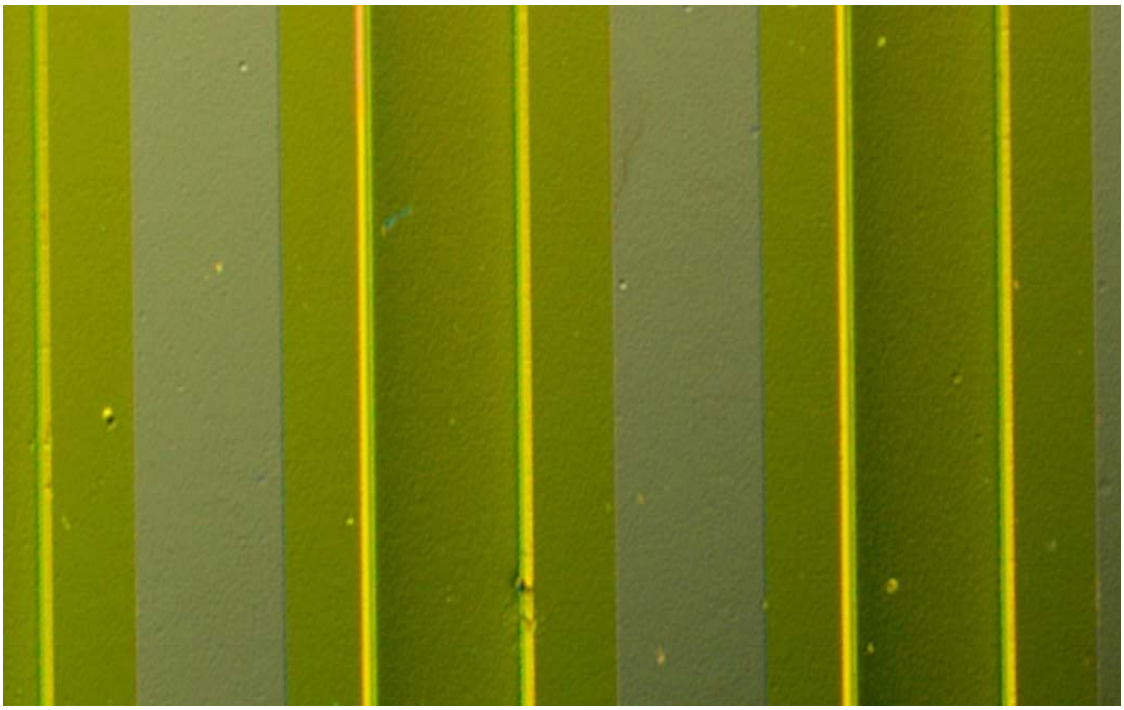

Figure 31: An image of the wafer with grooves processed by wet chemical etching. The contact areas have a grey coloration, while the similarly sized groove areas appear as a darker green.

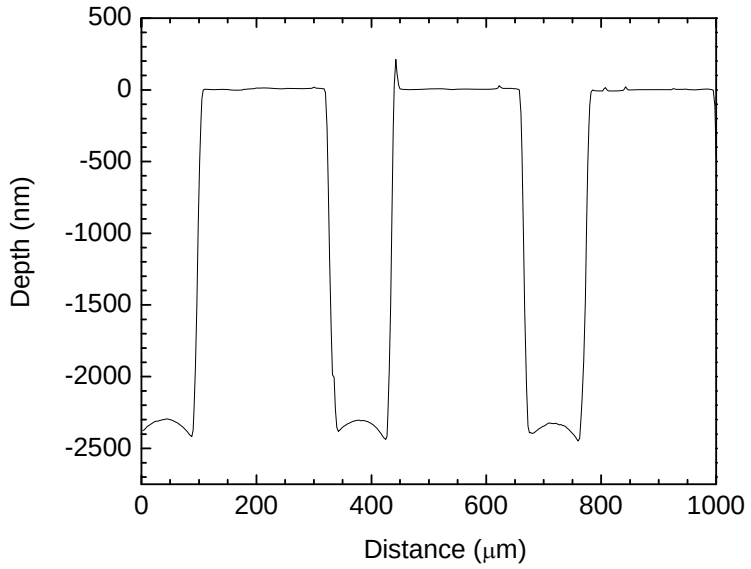

Figure 32: Depth profile of the etched grooves obtained with DEKTAK surface profiler.

A 1-mm-long bar was cleaved from the grooved wafer and mounted n-side down (uncoated) onto a copper heat sink in order to assess the laser operation and to verify suppression of the lateral mode generation. A near-field image of the array is shown in Figure 33.

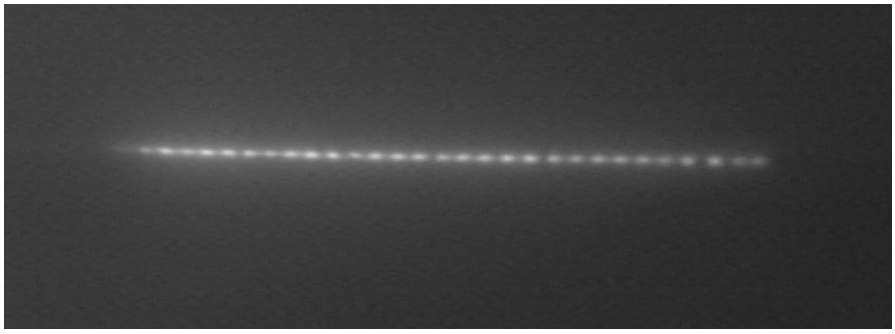

Figure 33: Near-field image of the laser diode array.

Figure 34 shows the emission spectrum of a 7-element portion of the bar cleaved from the same wafer. Since the devices were mounted n-side down, pulsed operation was required to avoid overheating. The smaller piece was tested in order to reduce the required current, making it possible to pump the arrays using our existing pulse

generator. A repetition rate of 100 kHz was utilized for spectrum measurements with the Nicolet Magna 860 continuous scan Fourier transform infrared (FTIR) spectrometer.

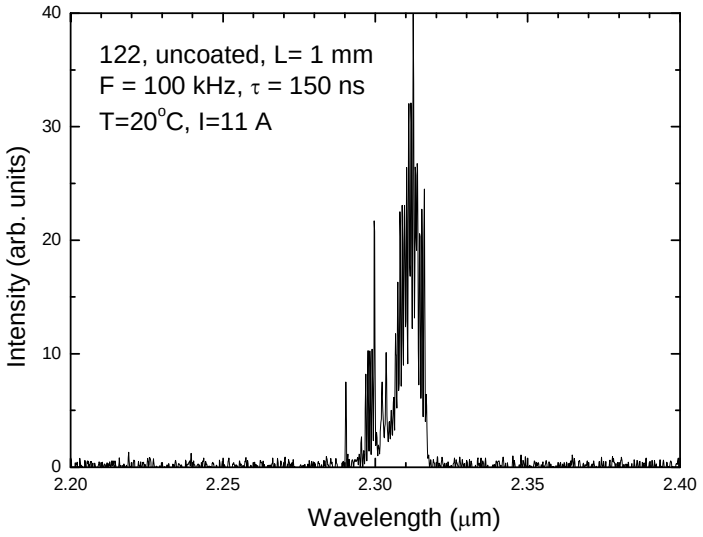

Figure 34: Emission spectrum of the laser material.

The emission spectrum is centered near 2.3 μm. The output power of the uncoated bar mounted n-side down was measured under pulsed mode operation (Figure 35). A peak power of 9 W was obtained from the uncoated arrays with no evidence of power saturation (significantly more power would be expected from a coated array).

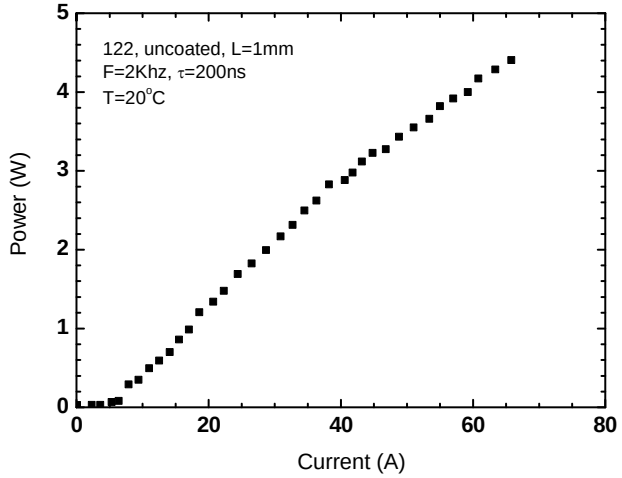

Figure 35: Peak output power (per facet) obtained from the uncoated laser diode array mounted n-side down onto a copper heat sink. The temperature was stabilized with a thermoelectric cooler.

5.1 Arrays with coated facets:

A grooved laser bar with 1 mm long cavities was coated with a high reflectivity (HR) coating on one facet and an anti-reflection (AR) coating on the other facet. A 4 mm segment of this bar, containing 12 individual laser apertures, was cleaved off and mounted via indium soldering onto a standard 'c' block. As expected, the AR/HR coated laser produced significantly more power from the output facet as compared to the uncoated device (Figure 36).

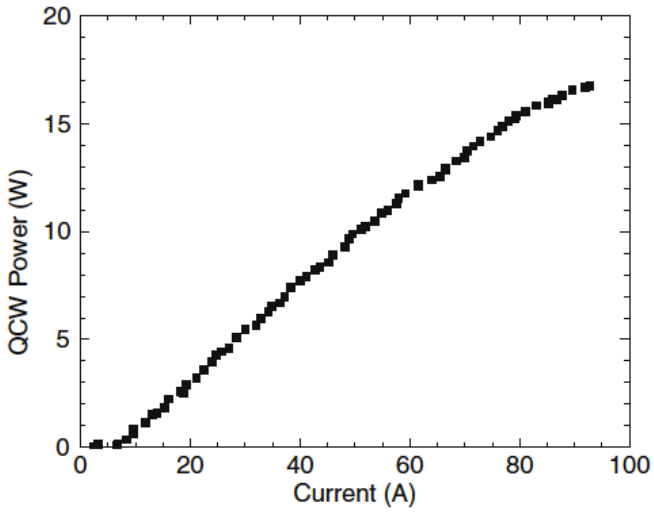

Figure 36: QCW (30 μs, 300 Hz) output power from an HR/AR coated laser array with 1-mm cavity length and 4-mm-wide emitting area. Measurements were performed at a heat sink temperature of 18 °C.

An initial slope efficiency of 0.235 W/A and a threshold current of 6.9 A were demonstrated. A qCW output power of 16.7 W was achieved.

This 4 mm array was the largest that could be comfortably mounted on a standard 'c' block. Scaled to the industry standard 10 mm laser bar length, this device would have produced 41.75 W of qCW output power at 18 °C.

6 Personnel Supported:

David Westerfeld, Gregory Belenky, Dmitry Donetsky, Mikhail Kisin, Sergey Suchalkin, Leon Shterengas, Takashi Hosoda, Jianfeng Chen and Alex Gourevitch are supported by or associated with this project.

7 Publications:

- L. Shterengas, G. Belenky, J.G. Kim, A. Gourevitch, D. Donetsky, D. Westerfeld, R. Martinelli, "Effect of compressive strain on differential gain of GaSb-based type-I QW lasers," oral presentation at Conference on Lasers and Electro-Optics, May 21-26 (2006) Long Beach, California, USA.

- L. Shterengas, G. Belenky, MV Kisin, D. Donetsky, "High power 2.4 μm heavily M. V. Kisin, L. Shterengas, J.G. Kim, G. Belenky, "Enhancement of Optical Gain in Sb-based MIR Diode Lasers", oral presentation at International Semiconductor Laser Conference, September 18-21 (2006) Kohala Coast, Hawaii, USA.

- L. Shterengas, G. Belenky, M. V. Kisin, D. Donetsky, "High power 2.4 μm heavily strained strained type-I quantum well GaSb-based diode lasers with more than 1 W of continuous wave output power and a maximum power-conversion efficiency of 17.5%", Applied Physics Letters, Jan 2007

- L.Shterengas, G. Belenky, M..V. Kisin, D. Donetsky, D. Westerfeld, "High power 2.4 μm Type–I QW GaSb-based diode lasers with enhanced differential gain", MIOMD-07, Bad Ischl, Austria, May 2007.

- Donetsky, L.Shterengas, M.V.Kisin, "Heavily strained InGaAsSb/AlGaAsSb quantum well heterostructures for optoelectronic applications", Electronics Material Conference, EMC -49, Notre-Dame University, IN, June 2007.

- D. Donetsky, G. Kipshidze, L. Shterengas, T. Hosoda, G. Belenky, "2.3 μm type-I quantum well GalnAsSb/AlGaAsSb/GaSb laser diodes with quasi-CW output power of 1.4W", Electronics Letters, Jul 2007

- L. Shterengas; G. Belenky; M. Kisin; D. Donetsky; D. Westerfeld, "Recent developments in high power 2.3-2.4 μm diode lasers", SPIE, 6552, Laser Source Technology for Defense and Security III (2007).

- D. Donetsky, J. Chen, L. Shterengas, G. Kipshidze, D Westerfeld, D, "2.3-mu m High-Power Type I Quantum-Well GaInAsSb/AlGaAsSb/GaSb Laser Diode Arrays with Increased Fill Factor", Journal Of Electronic Materials, Dec 2008

8 Interactions/Transitions:

There have been no interactions/transitions of this effort.

9 New Discoveries:

This work has been orientated to producing high power laser arrays emitting at 2.3 μm. In this we were successful, setting records for both individual laser and laser array output

power at this wavelength. The devices are also very practical: they operate at room temperature, with high stability, low production cost, compact dimensions, and high efficiency. Much of this work has involved refining pre-existing laser designs, and, as such there are limited opportunities for new discoveries. Several breakthrough developments have taken place in the course of this research though:

- A specific feature of GaIn(Al)AsSb alloys is the relatively low valence band offsets. We have shown that these offsets can be significantly improved by use of the heavily compressively strained GaInAsSb QW materials thanks to strain-induced upward shift of the QW valence band edge. Our calculations show that in contrast to strain-induced DOS balancing, which is efficient for strain values up to 1%, this mechanism remains efficient in GaSb-based materials at higher strain values up to 2%.
- A method to suppress lateral lasing in laser arrays involving etched grooves and silicon nitride passivation that extracts no penalties in terms of individual laser performance or efficiency.
- An optimized laser heterostructure was developed to reduce voltage drop and current leakage from the quantum wells. This approach is generally applicable to a wide range of semiconductor laser applications.

10 Interactions/Transitions:

Power Photonic has delivered lasers to BAE and Innovative Photonic Solutions for evaluation in a next generation countermeasures system.